Journal of Ionic Liquids xxx (xxxx) 100078

Contents lists available at ScienceDirect

Journal of Ionic Liquids

journal homepage: www.elsevier.com

Exploring binding affinity of 1-n-Alkyl-3-methylimidazolium chloride with iron porphyrin and electron uptake ability of the ionic liquid-FeP complex

Sudip Kumar Das, Jindal K. Shah *

School of Chemical Engineering, Oklahoma State University, Stillwater, OK, 74078, United States

ARTICLE INFO

Keywords:
Ionic liquids
Biodegradation
Porphyrin
Electronic structure calculations
DFT
Natural bond orbital analysis
Thermodynamics
Electrophilicity

ABSTRACT

Interaction of ionic liquids with iron porphyrin (FeP) arises in a number of application of ionic liquids such as dye-sensitized solar cells, batteries, and conversion of CO_2 to value-added products, etc. Furthermore, ionic liquid-FeP interactions are thought to be responsible for ionic liquid biodegradation and catalytic breakdown of ionic liquids. Despite the importance of ionic liquid-FeP interactions, there is a lack of information on what conformations ionic liquids adopt when presented to FeP and how thermo- dynamics of subsequent electron transfer reaction is affected. To begin to answer these questions, electronic structure calculations are performed to assess how the bind- ing propensity of the homologous series of 1-n-alkyl-3-methylimidazolium [$C_n$mim]Cl (n = 2, 4, 6, 8, 10) to FeP is affected as the alkyl chain length and the initial conformation of the cation presented to FeP are varied. The conceptual density functional theory framework is then invoked to compute the electrophilicity index of the ionic liquid-FeP complex to glean insight into the ability of the complex to acquire an electron. Calculations suggest two equally likely conformations of ionic liquids with similar Gibbs free energy change; however, the enthalpic and entropic contributions differ based on the conformation adopted by ionic liquids which in turn affects the subsequent electron transfer process. The importance of results is discussed in terms of experimentally observed alkyl chain length-dependent biodegradability of ionic liquids.

1. Introduction

Ionic liquids are substances composed entirely of cations and anions and can remain liq- uid under a wide range of temperatures. Their unique properties such as negligible vapor pressure, (Dong et al., 2017) low melting points, (Lei et al., 2017) high thermal and chemical stability, (Lei et al., 2017) and tuning for specific applications by selecting cations and anions from a vast chemical space, make this class of chemical promising for various chemical processes. For examples, ionic liquidss are at the forefront of industrial applications such as gas separation techniques, (Baltus et al., 2005) dye-sensitized solar cells, (Bousrez et al., 2021) battery electrolytes, (Zhou et al., 2021) electroplating and chromatography. (Chotkowski et al., 2020; Brown et al., 2018) More recently, several groups have suggested the use of binary and reciprocal ionic liquids in search for optimum physico-chemical and gas separation properties. (Dhakal et al., 2022; Fatima et al., 2020)

Though ionic liquids are classified as green solvents as a vast majority of them possess low vapor pressures, biodegradability of many ionic liquids remains a critical challenge. (Coleman and Gathergood, 2010; Jordan and Gathergood, 2015) Several excellent reviews provide a comprehensive analysis of various ionic liquid attributes such as cation head group, length of the alkyl chain length, the role of alkyl chain functional- ization, type of the anion and experimental conditions involving mixed microbial culture or specific strains of bacteria. Here, representative studies are included to highligh trends that have emerged over the last two decades. (Coleman and Gathergood, 2010; Jordan and Gathergood, 2015; Pham et al., 2010; de Jesus and Maciel Filho, 2022) Experiments have demonstrated that the length of the alkyl chain in imidazolium-based and pyridinium-based cations is a key determinant of the extent of biodegradation such that chains shorter than butyl are recalcitrant while partial to complete biodegradation can be observed for longer alkyl chain lengths. (Docherty et al., 2007) The extent of biodegradation was also found to depend on the type of the cationic core (Neumann et al., 2014; Abrusci et al., 2011) and the type of functional group substitutions. (Neumann et al., 2014; Gathergood et al., 2004) Varying effect of the anion has been found on biodegradation. For example, the work by Mena et al. shows that there is no effect of the anion on the biodegradation of 1-butyl-3-methylimidazolium, (Mena et al., 2020) while anion-dependent biodegradation was observed by Abursci et al. (Abrusci et al., 2011) The effectiveness of en-

* Corresponding author.
E-mail address: jindal.shah@okstate.edu (J.K. Shah).

https://doi.org/10.1016/j.jil.2024.100078
Received 23 November 2023; Received in revised form 13 February 2024; Accepted 13 February 2024
2772-4220/

riching microbial culture to trigger biodegradation of generally considered non-biodegradable ionic liquid has been reported in several studies as well. (Koutinas et al., 2019; Alisawi et al., 2017; Docherty et al., 2015; Deng et al., 2015)

Given that industrial applications of ionic liquids are on the rise, it is imperative to un- derstand molecular-level processes that contribute or hinder ionic liquid biodegradation in an effort to design ionic liquids that are inherently biodegradable yet deliver performance needed for the intended use. An analysis of metabolites produced as ionic liquids undergo biotransformation can yield important insights into biodegradation pathways and how they may be accelerated. Several experimental investigations have found that one of the primary metabolites contains an -OH moiety in the alkyl chain length, (Alisawi et al., 2017; Stolte et al., 2008; Pham et al., 2009; Zhang et al., 2011; Chua and Zhou, 2019; Liwarska-Bizukojc et al., 2015) which led several au- thors to suggest that the oxidation was catalyzed by mono-oxygenases such as cytochrome $_{P450.}$23,27

Although experimental evidence suggests that cytochrome P450, a superfamily of en- zymes containing iron porphyrin (FeP) acting as a catalytic site, may be implicated in the initial biotransformation of ionic liquids, currently there is no information on how ionic liquids bind in the enzymatic pocket. In addition, the overall hydroxylation reaction is com- prised of several intermediate steps. (Schlichting et al., 2000) However, there is complete lack of knowledge related to thermodynamics and kinetics of these steps, which hampers the understanding of rate- limiting or thermodynamically infeasible steps when shorter alkyl chains are accommodated in the binding pocket. In this manuscript, this knowledge gap is addressed for the first two steps in the hydroxylation cycle: the binding of the ionic liquid and subsequent transfer of electron to ionic liquid-FeP complex. In previous publications by Banerjee and Shah, the dependence of thermodynamics of these two steps on the alkyl chain length in the imida- zolium family (Banerjee and Shah, 2019) and for various ionic liquid cation classes (Banerjee and Shah, 2020) was investigated. These articles concluded that thermodynamic driving force existed for the first two steps. However, these studies did not consider the possibility that an anion may be present in the binding pocket. In this work, the effect of including an inorganic anion such as Cl^- on the thermodynam- ics of ionic liquid binding and the propensity for electron transfer to the complex is evaluated.

In the next section, methodological aspects are outlined with details on the influence of the initial conformations of the ionic liquid [$C_n$mim] Cl (n = 2, 4, 6, 8, 10) presented to FeP on the final optimized geometries using density functional theory (DFT) calculations. Thermo- dynamics of each of the conformations is evaluated in terms of Gibbs free energy change to determine the most stable geometry. The analysis is followed by decomposition of the Gibbs free energy change into enthalpic and entropic contributions to reveal molecular-level driving forces for the binding event. Using natural bond orbital theory, second-order perturbation energies are calculated for various donor-acceptor moieties in the complex to further dissect the origins of enthalpic differences for different conformations. A frontier orbital analysis is then carried out to obtain the propensity of the ionic liquid-FeP complex in acquiring an electron based on the conceptual density functional theory.

2. Methods

2.1. Computational details

In this study, 1-n-alkyl-3-methylimidazolium [$C_n$mim]$^+$ was considered as the cation with variable alkyl chain lengths (n = 2, 4, 6, 8, and 10) and chloride Cl^- as the anion. The gas phase geometries of cation, anion and FeP were optimized using Gaussian 09 software package. (Frisch et al., 2009) All the atoms except Fe were treated with Pople's medium 6-31G(d,p) basis set. (Hehre et al., 1972) LanL2DZ basis set was used for Fe as the basis set has been proven computationally efficient for transition metal containing systems. (Hay and Wadt, 1985) M06, an advanced hybrid meta-exchange- correlation function, was employed as the density functional theory for these calculations to account for non-local interactions that are likely to occur due to the presence of alkyl chains. (Zhao and Truhlar, 2008) As Fe can exist in multiple spin states, the geometry optimization was carried out at various spin states: singlet, triplet, and quintet; the lowest energy spin state was considered for subsequent analysis. A local minimum for the ionic liquid-FeP complex was confirmed by ensuring that the optimized structure did not contain any imaginary frequency.

2.2. Conformational-Dependent geometry optimization

In this work, geometry optimization was performed for two different orientations of ionic liquid cations with respect to porphyrin, viz. tail up and tail down, as these were identified to be the two widely different conformation from the previous work, (Banerjee and Shah, 2019) and various Cl^- positions relative to the ionic liquid cation. To account for relative orientation and placement of three species (FeP, cation, and anion), the initial positions of the molecules were identified using a spherical coordinate system with Fe at the origin. The XY plane of the coordinate system was aligned with that of FeP such that two adjacent nitrogen atoms were placed along the X and Y axes, respectively, while the Z-axis was oriented perpendicular to the Fe plane. The orientation of the cation was determined by placing either the carbon atom in the methyl position above Fe (tail up) or the terminal carbon atom in the alkyl chain facing Fe (tail- down) such that the Fe-C vector was oriented along the positive Z axis of the coordinate system. In both orientations, the distance between Fe and carbon atom was set to 4 ˚A. An example of the two conformations for [C_2mim]$^+$ is depicted in Fig. 1a and b. For the placement of the anion, spherical coordinate system R (distance from Fe), θ (the azimuthal angle), ϕ (the polar angle) was adopted (Fig. 1c). Several initial positions of Cl^- were probed by setting R = 7 ˚A while the values of θ were varied from 0○ to 360○ in 30○ interval and ϕ assumed the values of 30○, 60○, and 90○ yielding a total of 36 initial conformations for a given imidazolium orientation.

2.3. Gibbs free energy change

In order to determine the relative stability of tail-down and tail-up conformations, the Gibbs free energy change was computed for the binding process for each of the cation-anion pairs:

$$FeP + IonicLiquid \rightarrow ionicliquid - FeP \quad (1)$$

for which the Gibbs free energy change (ΔG) was evaluated using eq. 2

$$\Delta G = (\epsilon 0 + Gcorr) \times ionicliquid - FeP - (\epsilon 0 + Gcorr) \times FeP - (\epsilon 0 + Gcorr)\, Ionicliquid \quad (2)$$

where ϵ_0 is the electronic energy for a given species and G_{corr} refers to the thermal correction to the Gibbs free energy. The overall Gibbs free energy change was evaluated at 298.15 K. Enthalpic contributions (ΔH) to the Gibbs free energy change was determined in a similar manner (Eq. (3)).

$$\Delta H = (\epsilon 0 + Hcorr) \times ionicliquid - FeP - (\epsilon 0 + Hcorr) \times FeP - (\epsilon 0 + Hcorr)\, Ionicliquid \quad (3)$$

where H_{corr} represents the thermal correction to the enthalpy. The entropic contributions to the Gibbs free energy were evaluated from Eq. (4)

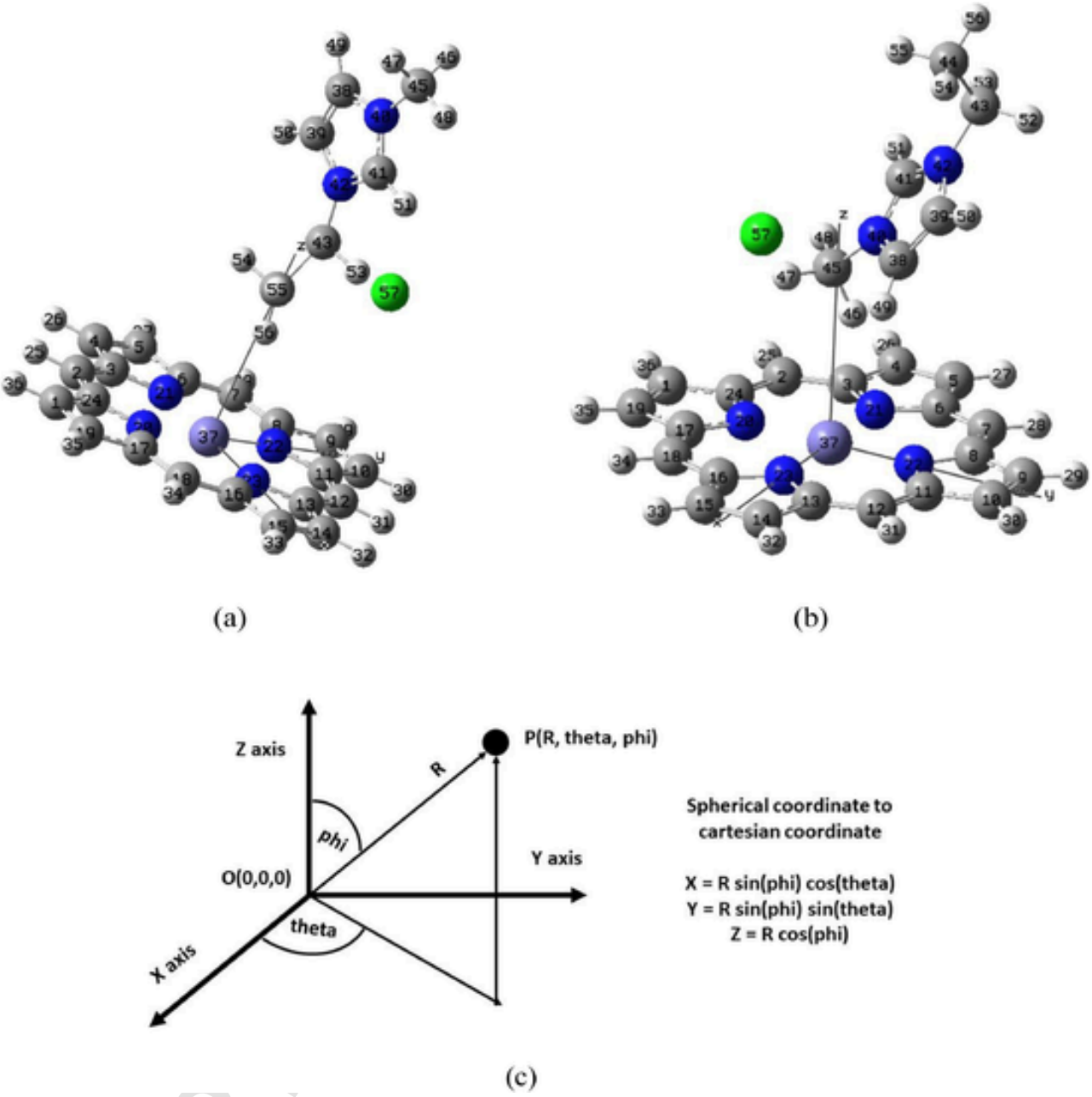

Fig. 1. (a)Typical initial orientation of tail down conformer for ionic liquid-FeP system for geometry optimization (b) Typical initial orientation of tail up conformer for ionic liquid-FeP system for geometry optimization (c) Typical spherical coordinate system and conversion of spherical coordinate to the Cartesian coordinate system.

$$\Delta S = \frac{\Delta H - \Delta G}{T} \tag{4}$$

where T is the temperature.

2.4. Global reactivity and site selectivity

The next step in the biodegradation cycle of ionic liquids, in the presence of FeP, is the addition of an electron to the system, which leads to the reduction of Fe^{3+} to Fe^{2+}. To understand the propensity of the ionic liquid-FeP complex to undergo the reduction process, global reactivity index, in terms of global electrophilicity index, and site selectivity for the electron addition were determined. The electrophilicity index for the whole system was computed by identifying the frontier molecular orbital energies using population analysis. Eqs. (5), 6, and 7 proposed by Parr et al. (1999) were used to compute the electrophilicity index for the whole complex.

$$\mu = \frac{E_{HOMO} + E_{LUMO}}{2} \tag{5}$$

$$\eta = E_{LUMO} - E_{HOMO} \tag{6}$$

$$\omega = \frac{\mu_2}{2\eta} \tag{7}$$

E_{HOMO} and E_{LUMO} indicate the energy of the highest occupied molecular orbital and the lowest unoccupied molecular orbital, respectively. μ, η, and ω refer to electron chemical potential, chemical hardness, and global electrophilicity index, respectively. In order to understand the reduction mechanism, the site selectivity of individual molecules within the complex was computed to identify the likelihood of a given atomic site to accept an electron. Local electrophilicity was computed

with the help of the Fukui function (f^+) from conceptual density functional theory using Eq. (6): (Chamorro et al., 2003; P´erez et al., 2002)

$$\omega_k = \omega f_k^+ \tag{8}$$

In Eq. (8), ω, ω_k, and f^+ are the global electrophilicity index, local electrophilicity, and con- densed Fukui function for nucleophilic attack, respectively. Condensed Fukui function for nucleophilic attack can be defined as eqs.: (Yang and Mortier, 1986)

$$f_k^+ = q_k(N+1) - q_k(N) \tag{9}$$

Here, $q_k(N+1)$, and $q_k(N)$ are the Hirshfeld charge analysis for the −1 and 0 charges of the ionic liquid-FeP complex, respectively. (Wang et al., 2019) In this work, Hirshfeld charge analysis was performed using the Multiwfn program. (Lu and Chen, 2012)

2.5. Natural bond orbital analysis

A detailed natural bond orbital (NBO) analysis, developed by Weinhold and co-workers, Glendening et al. (2012) was performed to understand the intramolecular and intermolecular interactions between the molecules within the complex. (Zhang et al., 2010) To identify dominant intramolecular and intermolecular charge delocalizations, calculations were carried out by considering possible interactions be- tween donor and acceptor from the second-order perturbation theory. For each type of NBO donor (i) and NBO acceptor (j), the second-order stabilization energy $E^{(2)}$ associated with i → j delocalization is estimated as

$$E^{(2)} = \Delta E_{ij}^{(2)} = q_i F_{ij}^{(2)} / \left(\epsilon_j - \epsilon_i\right) \tag{10}$$

In the above eq., q_i is the donor orbital occupancy, F_{ij} is the off-diagonal Fock matrix element, and ϵ_j, ϵ_i are the diagonal elements for orbital energies. For this work, second order delocalization energies were computed for four fragment: free base porphyrin (FBP), Fe, cation, and anion.

3. Results and discussion

3.1. Optimized geometries

The most stable configurations for each of the ionic liquid-FeP complexes starting from the two initial conformations are depicted in Fig. 2. It is evident from the figure that the starting tail down structures yield optimized structures in which the alkyl chain is parallel to the FeP plane, with the end of the alkyl chain exposed to Fe; the imidazolium ring, however, is progressively located away from Fe with an increase in the alkyl chain length. In contrast, when the alkyl chain is oriented away from Fe in the starting conformation, the optimized geometries are those in which the imidazolium ring is found to be parallel to the FeP plane with the alkyl chain continuing to point away from FeP.

To provide more quantitative picture of the orientations, several geometric metrics were computed, which are plotted in Fig. 3. The orientation of the imidazolium ring plane with respect to FeP was quantified in terms of the angle between the normal to FeP and that to the imidazolium ring as depicted in Fig. 3a. It can be observed that the values of the angle between the normals are nearly constant, irrespective of the alkyl chain length, for the tail-up starting configuration. Moreover, the values close to zero (between 3.8○ and 4.7○) confirm that the two planes are nearly parallel to each other as seen in Fig. 2 for these conforma- tions. On the other hand, the angle between the normals progressively increases as the alkyl chain becomes longer for the tail-down conformations reaching 90○ for [C_{10}mim], indicating that the imidazolium ring is nearly vertical with respect to the FeP plane. The positioning of the imidazolium ring, with respect to FeP, can be further understood by calculating the distance between Fe and the center-of-mass (COM) of the imidazolium ring as displayed in Fig. 3b. It is found that the distance between Fe and COM of the imidazolium ring is almost invariant as a function of the alkyl chain length for the tail-up conformations. As op- posed to this observation, there is a dramatic increase in the distance between Fe and COM of the imdiazolium ring in going from [C_2mim]Cl to [C_{10}mim]Cl. Taken together, it can be concluded that the tail-up conformations lead to optimized geometries in which imidazolium ring is located in proximity to FeP with its plane parallel to that of FeP and independent of the alkyl chain length, while the tail-down conformations result in optimized geometries in which the imidazolium ring adopts progressively tilted orientation with respect to FeP simultaneously and moving further from Fe as the alkyl chain length increases.

The position of the anion was quantified with respect to its distance from the acidic hy- drogen atom in the imidazolium ring (the hydrogen atom connected to the carbon atom bonded to two nitrogen atoms). Fig. 3c shows that this distance is nearly independent of the alkyl chain length. The close proximity of the anion (distance between 2 and 2.15 ˚A) suggests the presence of hydrogen bonding and that the presence of FeP is not destabilizing for the cation-anion interactions. The distance between Fe and Cl− remains constant for the tail up conformations, while it increases as the alkyl chain becomes longer, which can be explained on the basis that the imidazolium ring moves away from Fe, dragging Cl− with it due to the hydrogen bonding interactions (Fig. 3d).

3.2. Thermodynamics of ionic liquid binding to FeP

The Gibbs free energy change for each cation-anion pair in the two different starting config- uration is tabulated in Table 1 and shown in Fig. 4(a). The negative Gibbs free energy change for all the conforma-

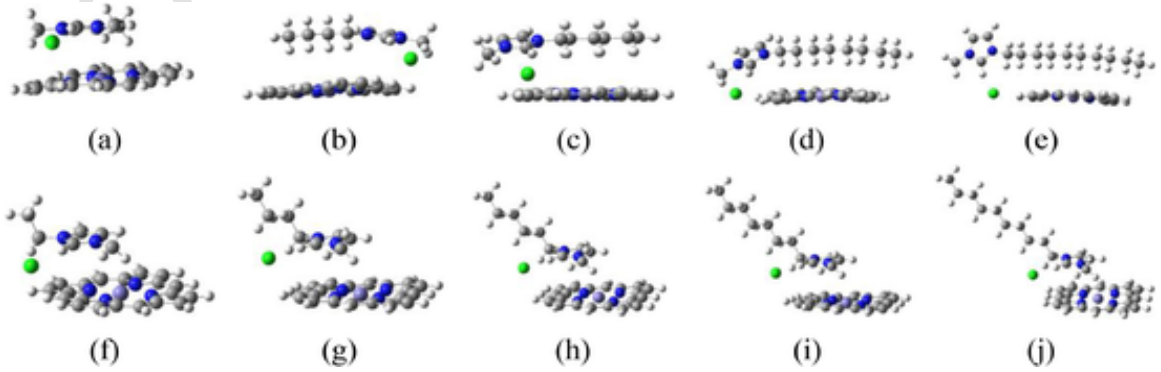

Fig. 2. Optimized geometries of the various ionic liquid-FeP complexes. The top pane depicts geometries observed for tail down starting conformations, while the bottom pane pro- vides final structures for tail up conformations. [C_2mim]$^+$ (a, f); [C_4mim]$^+$ (b, g); [C_6mim]$^+$ (c, h); [C_8mim]$^+$ (d,i); [C_{10}mim]$^+$ (e, j).

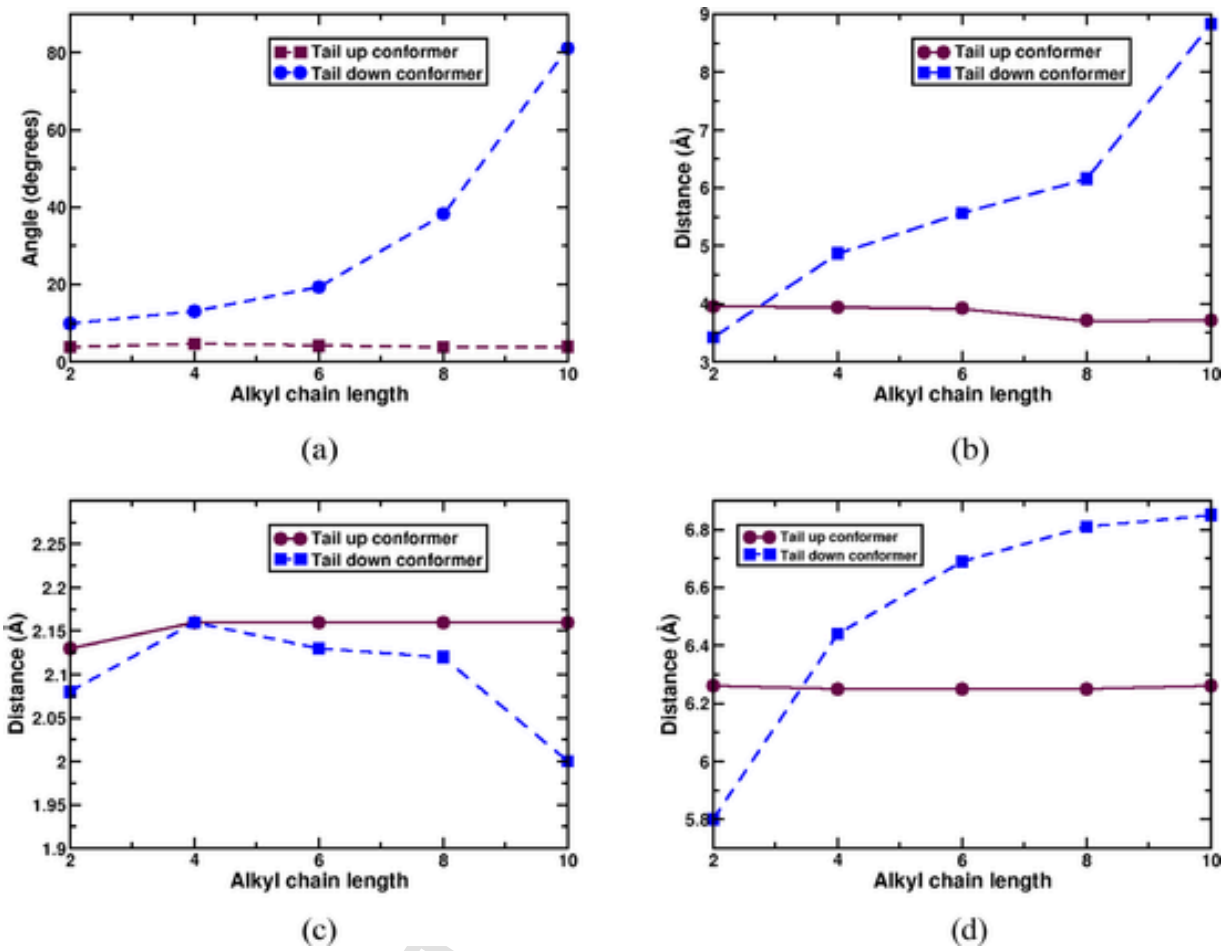

Fig. 3. (a) Angle between the normal to the FeP plane and the normal to the imidazolium ring plane; (b) distance between Fe and the center-of-mass of the imidazolium ring; (c) distance between the most acidic hydrogen atom in the imidazolium cation and Cl; (d) distance between Fe and Cl^{-}.

Table 1
Thermodynamics of ionic liquid binding to FeP.

Tail-up conformations			
Name of the Ionic liquid	ΔG (kcal/mol)	ΔH (kcal/mol)	ΔS (cal/mol K)
$[C_2mim]^+$	−12.1	−24.5	−41.5
$[C_4mim]^+$	−12.0	−23.7	−39.3
$[C_6mim]^+$	−10.6	−22.3	−39.4
$[C_8mim]^+$	−9.4	−21.3	−39.9
$[C_{10}mim]^+$	−13.7	−26.4	−42.7
Tail-down conformations			
Name of the Ionic liquid	ΔG (kcal/mol)	ΔH (kcal/mol)	ΔS (cal/mol K)
$[C_2mim]^+$	−14.3	−26.6	−41.0
$[C_4mim]^+$	−11.3	−24.8	−45.2
$[C_6mim]^+$	−11.1	−25.7	−48.9
$[C_8mim]^+$	−9.3	−25.5	−54.5
$[C_{10}mim]^+$	−14.0	−29.0	−50.3

tions indicate that the binding process is thermodynamically fea- sible, indicating that there is no thermodynamic barrier for the first step in the catalytic cycle for ionic liquid biodegradation. Furthermore, the binding free energy changes are within 1 kcal/mol, which can be regarded as chemical accuracy, for cations with alkyl chain $n \geq 4$, suggesting that there is no conformational preference when cations bind to FeP except possibly when $[C_2mim]Cl$ interacts with FeP. In this case, the equilibrium geometry start- ing from tail-down conformation is slightly favored. Based on the experimental observation that the hydroxyl group is inserted in the alkyl chain of the imidazolium-based cations and the existence of thermodynamic force for binding, it is likely that the conformations (c)-(e) in Fig. 2 are observed in the binding pocket of cytochrome P450, while conformations (f)-(j) support the incorporation of -OH in the imidazolium core. In order to delve deeper into the origin of the Gibbs free energy change, enthalpic and entropic contributions are collected in Table 1 and provided in Fig. 4(a) and (b), respectively. It can be observed that the enthalpic contributions favor the binding process while negative values for the en- tropy change suggest that there is a loss in entropy as ionic liquids bind to FeP opposing the binding process. As the entropic contributions are identical for tail-up and tail-down conformations for $[C_2mim]Cl$, the preference for the tail-down conformation originates from a greater enthalpic contribution. The entropic change is more or less constant for tail-up conformations (Fig. 2(f)-(j)), which can be rationalized based on almost identical orienta- tions adopted by the ionic liquid cation with respect to FeP. On the other hand, the entropy change becomes increasingly negative as the alkyl chain length increases for conformations shown in Fig. 2(a)-(e). The additional loss in the entropy is possibly due to the loss in conformational flexibility of the alkyl chain as it interacts with FeP. As remarked earlier, the free energy change is nearly identical for a given cation with $n \geq 4$, which implies that the increase in loss in the entropy disfavoring the binding process is compensated by the stronger enthalpic driving force for conformations displayed in Fig. 2(a)-(e). Thus, the present analysis provides a molecular-level understanding of how a subtle balance in the en- thalpic and entropic contributions leads to dramatic differences in the binding conformations of ionic liquids thereby influencing the site of reactivity.

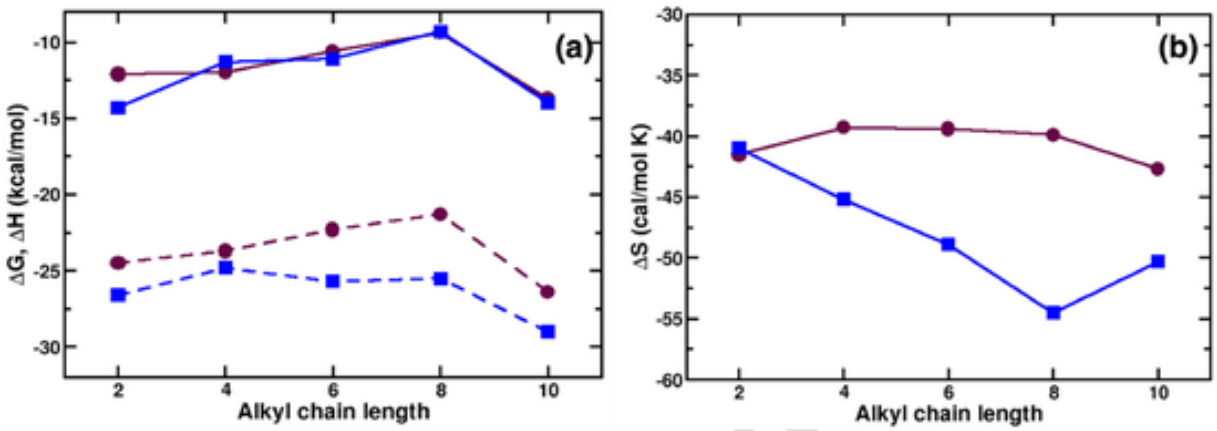

Fig. 4. (a) Gibbs free energy (solid line) and enthalpy change (dotted line) for ionic liquid binding to FeP (Eqs. (2) and (3) for tail-up (circles) and tail-down (squares) conformations; (c) entropy change (Eq. (4) for ionic liquid binding to FeP. Circles refer to the tail-up conformations while square identify tail-down conformations. Lines are provided as a guide to the eye.

3.3. Second-Order perturbation energy analysis

In order to explain the trends in enthalpic contributions reported above, second-order per- turbation analysis was performed decomposing a given ionic liquid-FeP system into four donor/acceptor fragments: free-base porphyrin (FBP), Fe, cation, and anion. All possible combinations of the donor-acceptor energy are tabulated in Tables 2 and 3 for tail-up and tail-down conformations, respectively. The non-zero donor-acceptor energies are plotted in Fig. 5. Enthalpic contributions arise due to interactions between the ionic liquid and FeP, e.g. FBP-cation, FBP-anion, Fe-cation, and Fe-anion. It can be observed that donation of the electronic density from the anion to FBP is considerably higher for tail-down confor- mations (Fig. 2(f)-(j)) for $n \geq 4$ than that for the corresponding tail-up conformations (Fig. 2(a)-(e)) which is correlated to the more negative enthalpy change for the former. Additional contribution arises due to the transfer of electronic density from FBP to cation, which is again higher in the case of tail-down conformations. Two-way interactions between Fe and cation are nearly identical for the two conformations. The data also shows there is no electronic interactions between Fe and anion. Thus, the higher enthalpy change for tail-down conformations originates due to the delocalization of electrons from anion to FBP and, to a certain extent, from FBP to the cation.

Table 2
Fragments-based energy analysis for tail-up conformers (Fig. 2(f)-(j)). Energies are in kcal/mol unit.

Fragments	$[C_2mim]^+$	$[C_4mim]^+$	$[C_6mim]^+$	$[C_8mim]^+$	$[C_{10}mim]^+$
FBP-Fe	331.39	333.01	332.58	331.20	332.31
FBP-cation	4.33	3.77	4.85	3.52	3.5
FBP-anion	0.0	0.09	0.0	0.0	0.0
Fe-FBP	82.98	91.32	91.06	83.04	90.79
Fe-cation	1.53	1.69	1.63	1.44	1.58
Fe-anion	0.0	0.0	0.0	0.0	0.0
cation-FBP	2.25	2.14	2.04	2.05	2.12
cation-Fe	0.81	0.86	0.95	0.84	0.92
cation-anion	0.17	0.12	0.12	0.12	0.12
anion-FBP	5.5	5.26	5.24	5.25	5.27
anion-Fe	0.0	0.0	0.0	0.0	0.0
anion-cation	31.85	29.49	29.33	29.34	29.31

Table 3
Fragments-based energy analysis for tail-down conformers (Fig. 2(a)-(e)). Ener- gies are in kcal/mol unit.

Fragments	$[C_2mim]^+$	$[C_4mim]^+$	$[C_6mim]^+$	$[C_8mim]^+$	$[C_{10}mim]^+$
FBP-Fe	314.31	327.75	317.57	318.86	308.71
FBP-cation	5.83	7.68	8.21	8.94	4.81
FBP-anion	0.08	0.0	0.0	0.0	0.0
Fe-FBP	69.05	93.55	70.17	68.98	73.00
Fe-cation	0.66	2.56	0.88	0.81	1.08
Fe-anion	0.09	0.0	0.0	0.0	0.0
cation-FBP	1.72	2.50	2.98	1.94	1.55
cation-Fe	2.94	0.87	1.16	1.28	2.02
cation-anion	0.18	0.16	0.16	0.18	0.18
anion-FBP	3.43	9.21	9.04	11.19	9.14
anion-Fe	0.0	0.0	0.0	0.0	0.0
anion-cation	35.39	32.35	33.63	36.09	32.18

3.4. Electrophilicity index

The next step in the ionic liquid biodegradation cycle is the reduction of the ionic liquid-FeP complex, the propensity for which can be estimated from the electrophilicity index (Eqs. 5, 6, and 7). Additionally, the local electrophilicity index was also determined to identify the most likely region for electrophilic attack making use of the condensed Fukui index and the Hirschfeld charge with Multiwfn. (Lu and Chen, 2012) Table 4 collects the electrophilicity index, condensed Fukui index, and the local electrophilicity index for the various cations and the two conform- ers. The global electrophilicity index are also displayed in Fig. 6.

For tail-up conformers, the electrophilicity index is the smallest for $[C_2mim]Cl$ and it in- creases by about 2 kcal/mol for $[C_4mim]Cl$. The propensity to acquire an electron stays constant with increasing alkyl chain length - the behavior stems from the fact that the HOMO and LUMO energies become invariant with the alkyl chain length for the tail-up conformers (Fig. S6a). The condensed Fukui index reveals that FeP is the most likely site for the addition of an electron as almost 95–96 % of the extra charge would be added to FeP, which can be rationalized based on the fact that the LUMO energy is located on FeP for all the conformers (Figs. S1b–S5b). In contrast to that for the tail-up conformers, the electron uptake ability for the ionic liquid-FeP complex diminishes with increase in the alkyl chain length. The decrease in the electron-uptake ability is gradual from $[C_2mim]Cl$ to $[C_8mim]Cl$ with a precipitous drop for $[C_{10}mim]Cl$. The behavior can be linked to a sharp decrease in the LUMO energy level from $[C_8mim]Cl$ to $[C_{10}mim]Cl$ (Fig. S6a). Furthermore, the movement of HOMO from Cl^- to FeP in $[C_{10}mim]Cl$ (compare Fig. S1a to Fig. S5a) is another reason that the addition of electron is energetically less favorable. It is interesting to note that the local electrophilicity index for FeP in $[C_{10}mim]Cl$-FeP complex is lower than that for bare FeP although the value of overall electrophilicity index still indicates that the electron addition to this system is possible. The electrophilicity index obtained in this study for the various conformers are significantly lower (almost 80–90 kcal/mol) than those reported by Banerjee and Shah for cation-FeP complexes.

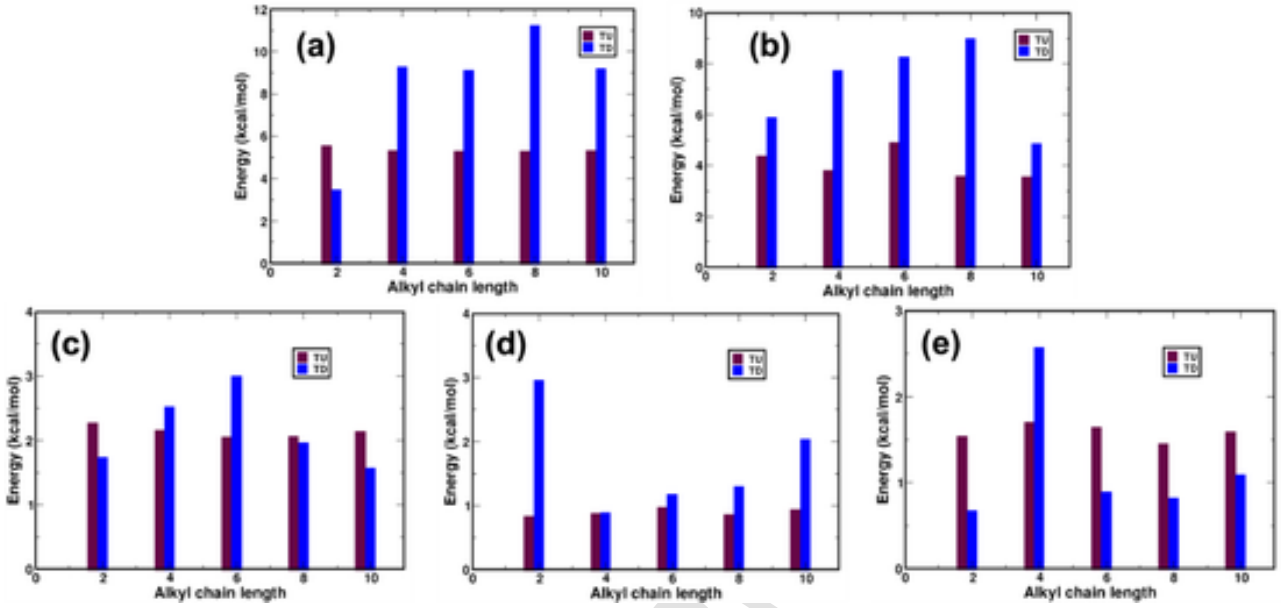

Fig. 5. Second order perturbation energy calculated from the NBO analysis. (a) anion- FBP; (b) FBP-cation; (c) cation-FBP; (d) cation-Fe; (e) Fe-cation. The first species is the donor fragment while the second refers to the acceptor fragment.

Table 4
Global and local electrophilicity index of two different types of conformers with iron porphyrin.

Name of the Ionic liquid	Global electrophilicity (ω), kcal/mol	Condensed Fukui index(f^+) k			Local Electrophicity index (ω_k),kcal/mol		
		FeP	Cation	Anion	FeP	Cation	Anion
Tail-up conformations							
$[C_2mim]^+$	64.07	0.95	0.03	0.022	60.87	1.92	1.41
$[C_4mim]^+$	65.96	0.96	0.022	0.02	63.32	1.45	1.32
$[C_6mim]^+$	65.96	0.96	0.022	0.02	63.32	1.45	1.32
$[C_8mim]^+$	65.96	0.96	0.022	0.02	63.32	1.45	1.32
$[C_{10}mim]^+$	65.96	0.96	0.022	0.02	63.32	1.45	1.32
Tail-down conformations							
$[C_2mim]^+$	65.75	0.94	0.04	0.025	61.81	2.63	1.64
$[C_4mim]^+$	64.31	0.95	0.027	0.02	61.09	1.74	1.29
$[C_6mim]^+$	61.42	0.93	0.056	0.018	57.12	3.44	1.11
$[C_8mim]^+$	59.91	0.92	0.06	0.017	55.12	3.59	1.02
$[C_{10}mim]^+$	48.87	0.93	0.065	0.004	45.45	3.18	0.20

(Banerjee and Shah, 2019) Although the electrophilicity index was calculated in a slightly different manner in the previous work, the primary reason for considerably lower propensity for acquiring electron is due to the presence of an anion which transfers electron density to FBP as revealed from the second-order perturbation en- ergy analysis.

In terms of ionic liquid biodegradability, local electrophilicity of the cation is of significant importance as it indicates which parts of the cations are most likely to undergo a reaction. Comparing this quantity along the homologous series and across the conformations indicates that the propensity for the cation to acquire the electron density from the electron transfer process is consistently higher for the tail-down conformations (Fig. 2) than that for the tail-up conformations. Furthermore, the local electrophilicity index for the cation increases with increase in the alkyl chain length for the tail-down conformations, which points to the fact that the cation is more likely to be activated the longer the alkyl chain length, which may partly explain biodegradation of ionic liquids bearing longer alkyl chain length.

4. Conclusion

Electronic structure calculations were carried out to understand the binding behavior of the ionic liquid $[C_nmim]Cl$ (n = 2, 4, 6, 8, 10) with FeP as this event is thought to be important for the first step in biodegradation of ionic liquids by cytochrome P450 enzyme. The Gibbs free energy change for the binding event is negative and more or less identical for the five systems irrespective of the starting configurations, suggesting that a given ionic liquid can exist in multiple conformations with implications on the final product formation. Decomposition of the Gibbs free energy change into its components revealed that the binding event is driven by enthalpy changes while entropy loss opposes the binding event. The second step of acquiring an electron in the hydroxylation cycle was also found to be thermodynamically feasible. In contrast to the binding step, the propensity for the electron transfer step depended signifi- cantly on the binding conformations adopted by the ionic liquid cation. The present study has thus demonstrated that one or more subsequent steps following the electron transfer re- action may be involved in exerting a control on the feasibility of the hydroxylation reaction and hence ultimately the biodegradability of imidazolium-based ionic liquids. Future work will focus on these aspects and how the implicit and explicit treatment of protein environ- ment and solvation will affect the subsequent steps for hydroxylation.

Although the interaction of ionic liquids with FeP was studied in the context of ionic liquid biodegradation, the understanding derived from this work can also be translated to advanced oxidation processes in which Fe-based catalysts are used to effectively break down ionic liquids containing aromatic cores, (Mena et al., 2022; Mena et al., 2019) which can aid in overcoming the lack of biodegradability of imidazolium-based ionic liquids. Several applications such as dye-sensitized solar cells, (Giri et al., 2014) oxidation of guanidoximes to cyanamides, (Kumari et al., 2015) conversion of CO_2 to value-added products, (Chen et al., 2017) polymerization, (Singhal and Ahmad, 2017) desulfurization of model fuels, (Zhao et al., 2017) and porphyrinic ionic liquid dyes, (Li et al., 2018) to name a few can benefit from a detailed understanding of molecular-level interactions of ionic liquid-porphyrin systems as described in this work.

The supporting information contains the HOMO and LUMO energy data used for the cal- culation of electrophilicity index.

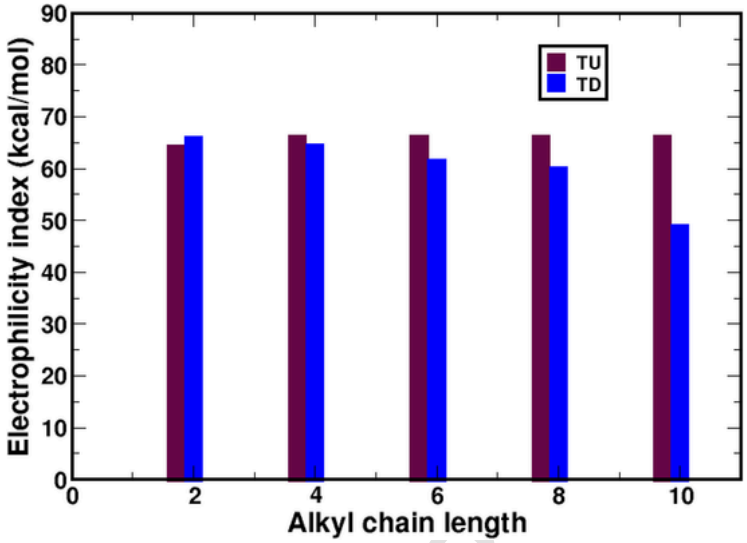

Fig. 6. Global electrophilicity index for tail-up and tail-down conformations.

CRediT authorship contribution statement

Sudip Kumar Das: Writing – review & editing, Writing – original draft, Methodology, Investigation. **Jindal K. Shah:** Writing – review & editing, Writing – original draft, Supervision, Resources, Project administration, Funding acquisition, Conceptualization.

Declaration of competing interest

The authors declare that they have no known competing financial interests or personal relationships that could have appeared to influence the work reported in this paper.

Data availability

Data will be made available on request.

Acknowledgement

Authors acknowledge funding for this work from the National Science Foundation Grant CBET-1845143. The computing for this project was performed at the High Performance Computing Center at Oklahoma State University supported in part through the National Science Foundation Grant OAC-1531128.

Supplementary materials

Supplementary material associated with this article can be found, in the online version, at doi:10.1016/j.jil.2024.100078.

References

Dong, K., Liu, X., Dong, H., Zhang, X., Zhang, S., 2017. Multiscale studies on ionic liquids. Chem. Rev. 117, 6636–6695.
Lei, Z., Chen, B., Koo, Y.M., MacFarlane, D.R., 2017. Introduction: ionic liquids. Chem. Rev. 117, 6633–6635.
Baltus, R.E., Counce, R.M., Culbertson, B.H., Luo, H., DePaoli, D.W., Dai, S., Duckworth, D.C., 2005. Examination of the potential of ionic liquids for gas separations. Sep. Sci. Technol. 40, 525–541.
Bousrez, G., Renier, O., Adranno, B., Smetana, V., Mudring, A.V., 2021. Ionic liquid-based dye-sensitized solar cells—insights into electrolyte and redox mediator design. ACS Sustain. Chem. Eng. 9, 8107–8114.
Zhou, W., Zhang, M., Kong, X., Huang, W., Zhang, Q., 2021. Recent advance in ionic-liquid-based electrolytes for rechargeable metal-ion batteries. Adv. Sci. 8, 2004490.
Chotkowski, M., Po·lomski, D., Czerwinski, K., 2020. Potential application of ionic liquids for electrodeposition of the material targets for production of diagnostic radioisotopes. Materials 13, 5069.
Brown, L., Earle, M.J., Gˆılea, M.A., Plechkova, N.V., Seddon, K.R., 2018. Ionic liquid–liquid chromatography: a new general purpose separation methodology. Ionic Liquids II 85–125.
Dhakal, P., Das, S.K., Shah, J.K., 2022. Revealing hydrogen bond dynamics between ion pairs in binary and reciprocal ionic liquid mixtures. J. Mol. Liq. 368, 120515.
Fatima, U., Dhakal, P., Shah, J.K., 2020. Comparative study of influence of ethanol and 2, 2, 2-trifluoroethanol on thermophysical properties of 1-ethyl-3-methylimidazolium di- cyanamide in binary mixtures: experimental and MD simulations. J. Chem. Eng. Data 66, 101–115.
Coleman, D., Gathergood, N., 2010. Biodegradation studies of ionic liquids. Chem. Soc. Rev. 39, 600–637.
Jordan, A., Gathergood, N., 2015. Biodegradation of ionic liquids–a critical review. Chem. Soc. Rev. 44, 8200–8237.
Pham, T.P.T., Cho, C.W., Yun, Y.S., 2010. Environmental fate and toxicity of ionic liquids: a review. Water Res. 44, 352–372.
de Jesus, S.S., Maciel Filho, R., 2022. Are ionic liquids eco-friendly? Renew. Sustain. Energy Rev. 157, 112039.
Docherty, K.M., Dixon, J.N.K., Jr, C.F.K., 2007. Biodegradability of imidazolium and pyridinium ionic liquids by an activated sludge microbial community. Biodegradation 18, 481–493.
Neumann, J., Steudte, S., Cho, C.W., Tho¨ming, J., Stolte, S., 2014. Biodegradability of 27 pyrrolidinium, morpholinium, piperidinium, imidazolium and pyridinium ionic liquid cations under aerobic conditions. Green Chem. 16, 2174–2184.
Abrusci, C., Palomar, J., Pablos, J.L., Rodr´ıguez, F., Catalina, F., 2011. Efficient biodegradation of common ionic liquids by Sphingomonas paucimobilis bacterium. Green Chem. 13, 709–717.
Gathergood, N., Garcia, M.T., Scammells, P.J., 2004. Biodegradable ionic liquids: part I. Concept, preliminary targets and evaluation. Green Chem. 6, 166–175.
Mena, I., Diaz, E., Palomar, J., Rodriguez, J., Mohedano, A., 2020. Cation and anion effect on the biodegradability and toxicity of imidazolium– and choline–based ionic liquids. Chemosphere 240, 124947.
Koutinas, M., Vasquez, M.I., Nicolaou, E., Pashali, P., Kyriakou, E., Loizou, E., Papadaki, A., Koutinas, A.A., Vyrides, I., 2019. Biodegradation and toxicity of emerging contaminants: isolation of an exopolysaccharide-producing Sphingomonas sp. for ionic liquids bioremediation. J. Hazard. Mater. 365, 88–96.
Alisawi, W.A., Rahbarirad, S., Walker, K.A., Venter, A.R., Docherty, K.M., Szym- czyna, B.R., 2017. Identification of metabolites produced during the complete biodegradation of 1-butyl-3-methylimidazolium chloride by an enriched activated sludge microbial com- munity. Chemosphere 167, 53–61.
Docherty, K.M., Aiello, S.W., Buehler, B.K., Jones, S.E., Szymczyna, B.R., Walker, K.A., 2015. Ionic liquid biodegradability depends on specific wastewater microbial consortia. Chemosphere 136, 160–166.
Deng, Y., Beadham, I., Ghavre, M., Gomes, M.F.C., Gathergood, N., Husson, P., L´egeret, B., Quilty, B., Sancelme, M., Besse-Hoggan, P., 2015. When can ionic liquids be considered readily biodegradable? Biodegradation pathways of pyridinium, pyrrolidinium and ammonium-based ionic liquids. Green Chem. 17, 1479–1491.
Stolte, S., Abdulkarim, S., Arning, J., Blomeyer-Nienstedt, A.K., Bottin-Weber, U., Matzke, M., Ranke, J., Jastorff, B., Tho¨ming, J., 2008. Primary biodegradation of ionic liquid cations, identification of degradation products of 1-methyl-3-octylimidazolium chloride and electrochemical wastewater treatment of poorly biodegradable compounds. Green Chem. 10, 214–224.
Pham, T.P.T., Cho, C.W., Jeon, C.O., Chung, Y.J., Lee, M.W., Yun, Y.S., 2009. Identification of metabolites involved in the biodegradation of the ionic liquid 1-butyl-3- methylpyridinium bromide by activated sludge microorganisms. Environ. Sci. Technol. 43, 516–521.
Zhang, C., Malhotra, S.V., Francis, A.J., 2011. Toxicity of imidazolium- and pyridinium-based ionic liquids and the co-metabolic degradation of N-ethylpyridinium tetrafluo-

roborate. Chemosphere 82, 1690–1695.
Chua, F.J.D., Zhou, Y., 2019. The role of ammonium oxidising bacteria (AOB) in ionic liquid 1-dodecylpyridinium chloride removal. Appl. Microbiol. Biotechnol. 103, 4595–4604.
Liwarska-Bizukojc, E., Maton, C., Stevens, C.V., 2015. Biodegradation of imidazolium ionic liquids by activated sludge microorganisms. Biodegradation 26, 453–463.
Schlichting, I., Berendzen, J., Chu, K., Stock, A.M., Maves, S.A., Benson, D.E., Sweet, R.M., Ringe, D., Petsko, G.A., Sligar, S.G., 2000. The catalytic pathway of cy- tochrome P450cam at atomic resolution. Science 287, 1615–1622.
Banerjee, A., Shah, J.K., 2019. Insight into conformationally-dependent binding of 1-n-alkyl- 3-methylimidazolium cations to porphyrin molecules using quantum mechanical calcu- lations. Phys. Chem. Chem. Phys. 21, 10095–10104.
Banerjee, A., Shah, J.K., 2020. Elucidating the effect of the ionic liquid type and alkyl chain length on the stability of ionic liquid–iron porphyrin complexes. J. Chem. Phys. 153, 1–12.
Frisch, M.J., et al., 2009. Gaussian 09 Revision C.01. Gaussian Inc, Wallingford CT.
Hehre, W.J., Ditchfield, R., Pople, J.A., 1972. Self-consistent molecular orbital methods. XII. Further extensions of Gaussian-type basis sets for use in molecular orbital studies of organic molecules. J. Chem. Phys. 56, 2257–2261.
Hay, P.J., Wadt, W.R., 1985. Ab initio effective core potentials for molecular calculations. Potentials for the transition metal atoms Sc to Hg. J. Chem. Phys. 82, 270–283.
Zhao, Y., Truhlar, D.G., 2008. The M06 suite of density functionals for main group ther- mochemistry, thermochemical kinetics, noncovalent interactions, excited states, and transition elements: two new functionals and systematic testing of four M06-class func- tionals and 12 other functionals. Theor. Chem. Acc. 120, 215–241.
Parr, R.G., Szentp´aly, L.v., Liu, S., 1999. Electrophilicity index. J. Am. Chem. Soc. 121, 1922–1924.
Chamorro, E., Chattaraj, P.K., Fuentealba, P., 2003. Variation of the electrophilicity index along the reaction path. J. Phys. Chem. A 107, 7068–7072.
P´erez, P., Toro-Labb´e, A., Aizman, A., Contreras, R., 2002. Comparison between experimental and theoretical scales of electrophilicity in benzhydryl cations. J. Org. Chem. 67, 4747–4752.
Yang, W., Mortier, W.J., 1986. The use of global and local molecular parameters for the analysis of the gas-phase basicity of amines. J. Am. Chem. Soc. 108, 5708–5711.
Wang, B., Rong, C., Chattaraj, P.K., Liu, S., 2019. A comparative study to predict regiose- lectivity, electrophilicity and nucleophilicity with Fukui function and Hirshfeld charge. Theor. Chem. Acc. 138, 1–9.
Lu, T., Chen, F., 2012. Multiwfn: a multifunctional wavefunction analyzer. J. Comput. Chem. 33, 580–592.
Glendening, E.D., Landis, C.R., Weinhold, F., 2012. Natural bond orbital methods. Wiley Interdiscipl. Rev.: Comput. Mol. Sci. 2, 1–42.
Zhang, Q.G., Wang, N.N., Yu, Z.W., 2010. The hydrogen bonding interactions between the ionic liquid 1-ethyl-3-methylimidazolium ethyl sulfate and water. J. Phys. Chem. B 114, 4747–4754.
Mena, I.F., Diaz, E., Rodriguez, J.J., Mohedano, A.F., 2022. An overview of ionic liq- uid degradation by advanced oxidation processes. Crit. Rev. Environ. Sci. Technol. 52, 2844–2887.
Mena, I.F., Diaz, E., P´erez-Far´ias, C., Stolte, S., Moreno-Andrade, I., Rodriguez, J.J., Mohedano, A.F., 2019. Catalytic wet peroxide oxidation of imidazolium-based ionic liquids: catalyst stability and biodegradability enhancement. Chem. Eng. J. 376, 120431.
Giri, N.K., Banerjee, A., Scott, R.W.J., Paige, M.F., Steer, R.P., 2014. Spectroscopic and photophysical study of the demetallation of a zinc porphyrin and the aggregation of its free base in a tetraalkylphosphonium ionic liquid. Phys. Chem. Chem.Phys. 16, 26252–26260.
Kumari, P., Nagpal, R., Chauhan, P., Yatindranath, V., Chauhan, S.M.S, 2015. Efficient iron(III) porphyrins-catalyzed oxidation of guanidoximes to cyanamides in ionic liquids. J. Chem. Sci. 127, 13–18.
Chen, Y., Luo, R., Yang, Z., Zhou, X., Ji, H., 2017. Imidazolium-based ionic liquid decorated zinc porphyrin catalyst for converting CO_2 into five-membered heterocyclic molecules. Sustain. Energy Fuels 2, 125–132.
Singhal, A., Ahmad, S., Chauhan, S.M.S., 2017. Iron(III) porphyrin catalyzed ionic liq- uid mediated polymerization of methylmethacrylate. Appl. Organomet. Chem. 32, e4044–e4046.
Zhao, R., Wang, J., Zhang, D., Sun, Y., Han, B., Tang, N., Zhao, J., Li, K., 2017. Deep catalytic oxidative desulfurization of model fuel based on modified iron porphyrins in ionic liquids: anionic ligand effect. ACS Sustain. Chem. Eng. 5, 2050–2055.
Li, K., Titi, H.M., Berton, P., Rogers, R.D., 2018. Porphyrinic ionic liquid dyes: synthesis and characterization. ChemistryOpen 7, 659–663.